THE JOURNAL OF PHYSICAL CHEMISTRY Letters

Letter

pubs.acs.org/JPCL

Chromophores in Molecular Nanorings: When Is a Ring a Ring?

Patrick Parkinson,*[,†] Dmitry V. Kondratuk,[‡] Christopher Menelaou,[†] Juliane Q. Gong,[†] Harry L. Anderson,[‡] and Laura M. Herz*[,†]

[†]Department of Physics, University of Oxford, Clarendon Laboratory, Parks Road, Oxford OX1 3PU, United Kingdom

[‡]Department of Chemistry, University of Oxford, Chemistry Research Laboratory, 12 Mansfield Road, Oxford OX1 3TA, United Kingdom

Supporting Information

ABSTRACT: The topology of a conjugated molecule plays a significant role in controlling both the electronic properties and the conformational manifold that the molecule may explore. Fully π-conjugated molecular nanorings are of particular interest, as their lowest electronic transition may be strongly suppressed as a result of symmetry constraints. In contrast, the simple Kasha model predicts an enhancement in the radiative rate for corresponding linear oligomers. Here we investigate such effects in linear and cyclic conjugated molecules containing between 6 and 42 butadiyne-linked porphyrin units (corresponding to 600 C−C bonds) as pure monodisperse oligomers. We demonstrate that as the diameter of the nanorings increases beyond ∼10 nm, its electronic properties tend toward those of a similarly sized linear molecule as a result of excitation localization on a subsegment of the ring. However, significant differences persist in the nature of the emitting dipole polarization even beyond this limit, arising from variations in molecular curvature and conformation.

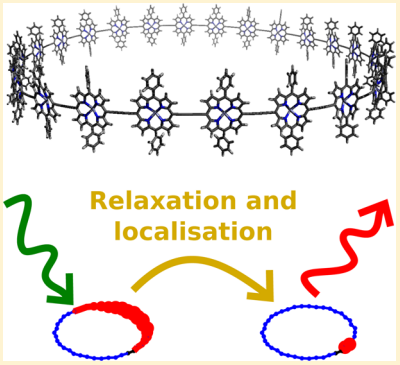

SECTION: Spectroscopy, Photochemistry, and Excited States

Control over the physical shape of conjugated polymers provides an intriguing possibility to isolate and investigate the impact of molecular topology on exciton behavior.[1] Cyclic molecules can exhibit profoundly different dynamics to their linear counterparts[2,3] both through symmetry-enforced radiative rate suppression[4] and thermally activated superradiance[5] and through a reduction in the size of the conformational manifold that the molecule may explore.[6] Within the conventional Kasha model,[7,8] radiative rate suppression (for nanorings) or enhancement (for linear oligomers) is analogous to the formation of H (or J) aggregates, respectively.[9,10]

Exciton delocalization around a cyclic structure is known to lead to a strong suppression of the fluorescence, for instance, in benzene.[11] Such delocalization has been shown to play an essential role in chlorophyll-based natural light-harvesting systems[12−14] and is often observed as an ultrafast drop in fluorescence anisotropy.[4] However, as the ring sizes increases a fundamental question arises: when the local environment experienced by an excitation spans just a subsegment of the cyclic molecule, do its emissive properties reflect those of a molecular ring or of a linear chain?

In this study, we address the relationship between molecular topology and exciton delocalization dynamics. We report a synthetic approach to linear conjugated porphyrin oligomers, which provides excellent control over chain length from 6 to 42 repeat units; furthermore, by exploiting supramolecular Vernier-templating, cyclic nanorings were produced with a similar number of repeat units.[6,15−17] Large porphyrin nanorings have already been shown to exhibit fundamentally different folding properties to linear chains,[6] and have been used to investigate energy transfer in biomimetic systems.[18]

By investigating both photoluminescence (PL) polarization anisotropy dynamics[2] and PL radiative rate, we probe the extent and spatial arrangement of photoexcited excitons as a function of molecular size and topology. We have recently shown that nanorings with fewer than 24 butadiyne-linked porphyrin units (<30 nm circumference) show a reduction in radiative rate and ultrafast (<200 fs) emission depolarization relative to their linear counterparts indicative of exciton delocalization over the full nanoring within the duration of the exciting pulse.[5] Here we show that as we go beyond this size range, toward larger rings with up to 40 porphyrin units, the absorbing states begin to show clear signs of localization on part of the ring. Such large nanorings show anisotropy dynamics that qualitatively tend toward their linear counterparts. Monte Carlo conformation and exciton dynamics simulation demonstrate that the gradual shift from fully delocalized absorbing and emitting states for small rings ($N \approx 6$) is followed by a transitional range for intermediate ring sizes ($6 < N < 30$) for which the absorbing state is still delocalized but emission occurs from localized states. For the very largest rings ($N \geq 30$), localization is found to occur in both absorption and emission. Intriguingly, the quantitative exciton dynamics remain different from those observed for

Received: October 20, 2014
Accepted: November 20, 2014
Published: November 20, 2014

   dx.doi.org/10.1021/jz5022153 | J. Phys. Chem. Lett. 2014, 5, 4356−4361

linear molecules even for the largest nanorings studied, revealing a persistent role of topology on energy dynamics, as confirmed using Monte Carlo conformational and exciton dynamics simulation.

Large monodisperse butadiyne-linked porphyrin oligomers were prepared in both linear and cyclic (nanoring) topologies (Figure 1). Nanorings were made using classical[19] and

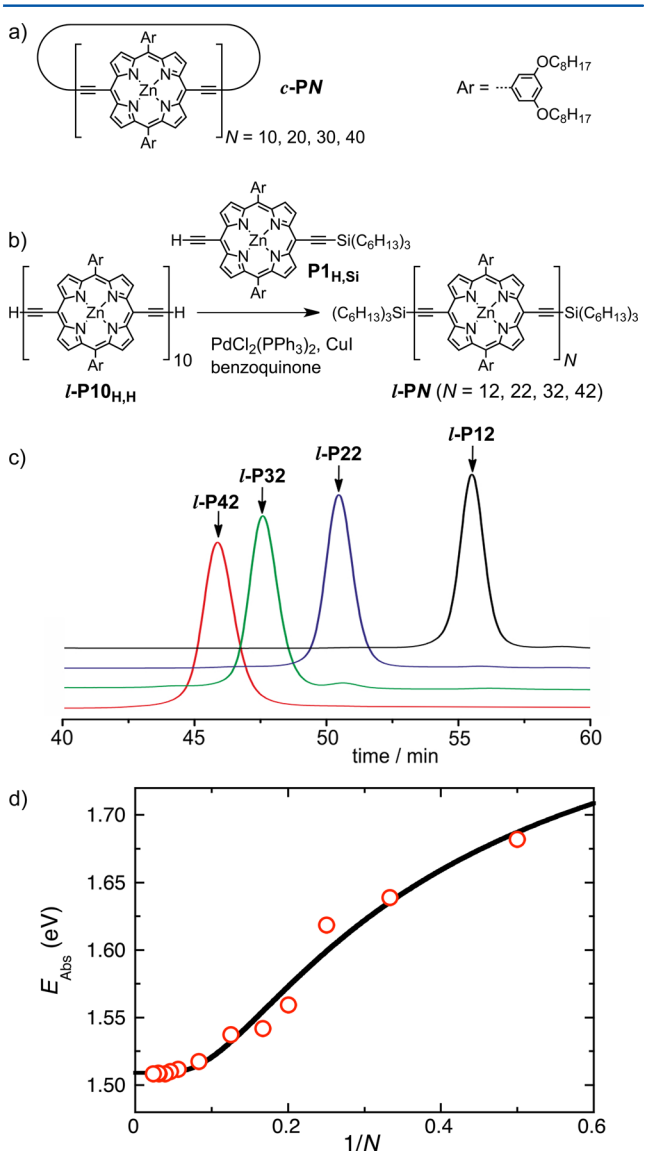

Figure 1. (a) Chemical structures of cyclic porphyrin oligomers ***c*-P*n***. (b) Synthesis of linear oligomers ***l*-P*n***. (c) Analytical GPC traces (toluene/1% pyridine, detection at 500 nm) of ***l*-P12**, ***l*-P22**, ***l*-P32**, and ***l*-P42**. (d) Meier plot of peak absorption energy against inverse number of repeat units for a range of linear porphyrin molecules from ***l*-P2** to ***l*-P42** (toluene/1% pyridine). The solid line is a fit as described in the text.

Vernier[6,17] template-directed synthesis, while linear oligomers of 12, 22, 26, 32, 34, and 42 porphyrin units were made by the novel synthetic approach shown in Figure 1b. The synthesis was achieved by palladium-catalyzed oxidative coupling[20] of the corresponding fully deprotected forms of linear porphyrin octamer ***l*-P8** or linear porphyrin decamer ***l*-P10** with a large excess of the singly capped porphyrin monomer. The resulting mixtures of oligomers were separated by recycling gel permeation chromatography (GPC). Their purity and identity were confirmed by ^{1}H NMR, MALDI-ToF, and GPC. (See Figure 1c and Supporting Information.) The energies of the absorption maxima of the linear oligomers with 2 to 42 porphyrin units are plotted against the reciprocal of the number of porphyrins in Figure 1d. This curve shows a saturation at about 20 porphyrin units, corresponding to an effective conjugation length[21] of ca. 27 nm, which is long compared with most other conjugated oligomers;[22−24] for instance, polythiophenes have been shown to have an effective conjugation length of between 4[25] and 16 nm.[21]

All optical experiments were carried out at room temperature in a toluene/1% pyridine (v/v%) solvent. Steady-state absorption and PL measurements were used to establish the basic photophysical properties and to confirm the strong conjugation of the porphyrin oligomers,[26] while fluorescence quantum yield and time-resolved PL measurements were employed to determine the radiative rates[27] (data in the Supporting Information).

Time-resolved PL spectroscopy was performed using an up-conversion technique. The sample was excited using ultrafast 780 nm (1.59 eV) laser pulses with a fluence of 125 pJ/pulse, creating excitons in the Q_x band. (See the absorption spectra in the Supporting Information.) Emission was monitored at 860 nm (1.44 eV) for all samples. This wavelength is close to the peak emission for all samples except for the shortest linear oligomers ***l*-P6**; however, we note that there is little difference in anisotropy for off-peak detection.[5] Typical PL decays for each sample are given in the Supporting Information.

PL polarization anisotropy is calculated using

$$\gamma(t) = \frac{I_{\mathrm{para}}(t) - I_{\mathrm{perp}}(t)}{I_{\mathrm{para}}(t) + 2I_{\mathrm{perp}}(t)} \quad (1)$$

where I_{para} and I_{perp} are the PL intensities measured with detection polarization parallel and perpendicular to the excitation pulse polarization, respectively. Several conceptually important cases have well-defined values for γ.[28] Short, linear oligomers typically exhibit $\gamma = 0.4$, indicating that the exciton transition dipole does not reorient following excitation.[29] Molecules that support free reorientation of the transition dipole in a 2D plane show $\gamma = 0.1$, as is the case for molecules with high 2D rotational symmetry.[2,3,30] Finally, molecules that support complete, 3D reorientation from the originally excited dipole transition ought to display $\gamma = 0$. Molecules such as the smaller nanoring systems presented typically have $\gamma \leq 0.1$,[4] arising from disorder-induced deviation of the molecule from perfect two-dimensionality, while linear chains show a dynamic reduction in anisotropy as the exciton migrates from its photogeneration site to a random orientation set by the chain conformation.[31,32]

Three aspects of the time-resolved anisotropy are particularly useful. The value of the PL anisotropy within the first ∼200 fs after excitation describes the relationship between the initially created and relaxed/self-localized exciton. The late-time anisotropy (after ca. 20 ps) is related to the eventual reorientation of the emissive exciton from its initially generated position. Lastly, the PL anisotropy dynamics provide information on the local environment of the exciton, specifically the curvature and diffusion or transport mechanism. Over a longer time scale, molecular reorientation in solution leads to all samples having a low PL anisotropy value ($\gamma \approx 0$); for this reason, we restrict our measurements to the first 20 ps, where

dx.doi.org/10.1021/jz5022153 | J. Phys. Chem. Lett. 2014, 5, 4356−4361

rotational diffusion is minimal. (See the Supporting Information for measurements over a larger time window.)

The time-dependent PL polarization anisotropy of all cyclic and linear oligomers is shown in Figure 2, while the initial

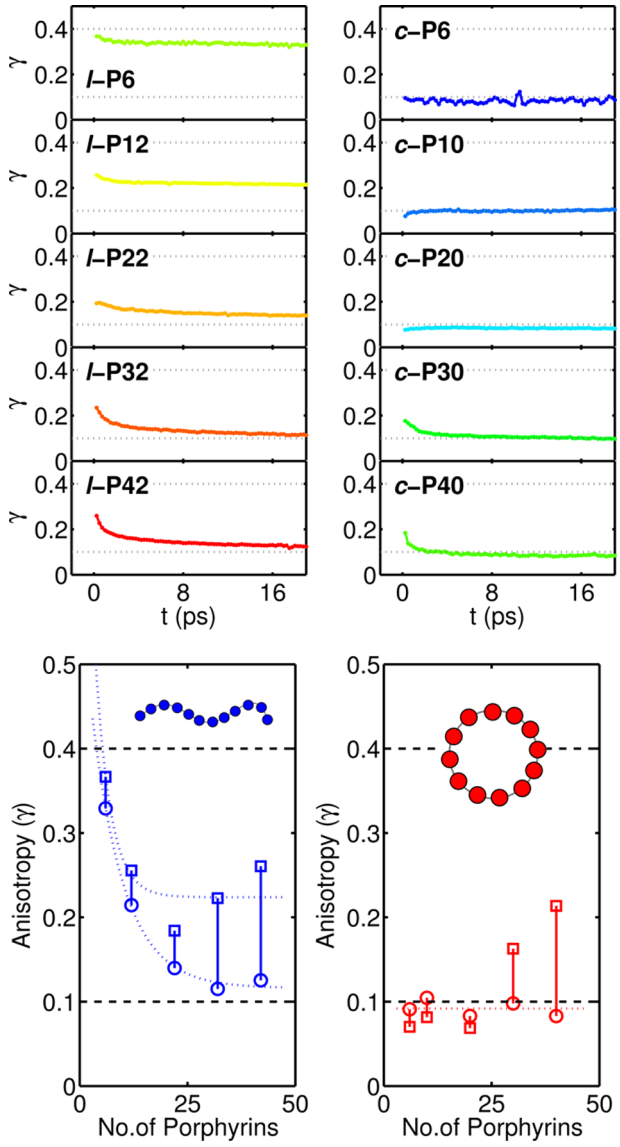

Figure 2. (Top) Time-resolved photoluminescence anisotropy for all samples. Note, the relatively large noise level for ***c*-P6** is caused by a low photoluminescence quantum efficiency for this molecule. Systematic errors were reduced by making multiple independent measurements of the anisotropy value. Dotted lines indicate key values of $\gamma = 0.4$ and 0.1 for polarization maintaining and 2D depolarization, respectively. (Bottom) Summary of anisotropy values for all samples. Squares shows the initial anisotropy value, while circles shows the value at $t = 20$ ps. A larger uncertainty is inherent for the initial anisotropy due to the steeper gradient in anisotropy at the earliest times. Dotted lines are a guide to the eye.

($t = 0$ ps) and late time ($t = 20$ ps) values of the anisotropy are summarized in the lower panel of the figure. Nanorings with 20 or fewer porphyrin units show an ultrafast and complete depolarization in two dimensions, as indicated by a value of $\gamma(t = 0\ \text{ps}) \leq 0.1$, in agreement with previous studies,[2,4,5] indicating an ultrafast loss of polarization memory due to exciton delocalization over the full nanoring. Conversely, linear chains of any size show a fast initial drop in anisotropy from values of between 0.2 and 0.4, followed by a picosecond decay. Strikingly, as the nanorings exceed 20 porphyrin units, the anisotropy dynamics begin to mirror the behavior observed for the linear chains with a clear decay dynamic indicative of excitons migrating along the molecule. One distinct difference remains: the value of γ drops to $\leq$0.1 more rapidly for the cyclic molecules, which we discuss later.

PL anisotropy provides information on the relative orientation of the initially excited and emissive exciton dipole direction and hence the delocalization of the absorbing state, while the radiative rate is a sensitive probe of the delocalization in the emissive state. In the Kasha model,[7] the lowest lying fully delocalized exciton state in a cyclic molecule is expected to have no net transition strength, whereas the transition strength of linear chains are expected to scale with chain length. Assuming that excitons relax to the lowest lying energy level available over the femtosecond time scale, the radiative rate for a molecule is a good measure of this transition strength. Figure 3 shows this

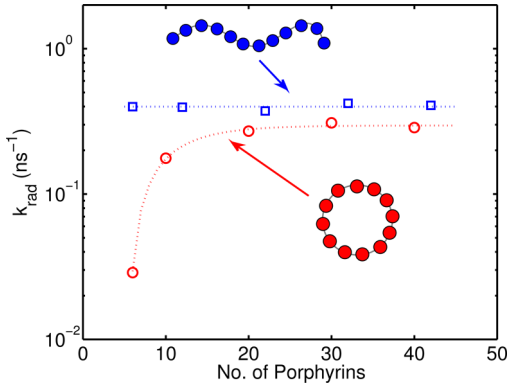

Figure 3. Radiative rate calculated using experimentally determined quantum efficiency (ϕ) and overall decay lifetime (τ) (data not shown, see Supporting Information). Blue squares show data for the linear molecules, while red circles show the data for the cyclic nanorings. Dotted lines are a guide to the eye.

rate for the linear molecules and nanorings, where the radiative rate k_r is calculated using the PL quantum yield ϕ and overall PL lifetime τ, via $k_r = \phi/\tau$. (See the Supporting Information for full details.)

We have previously shown that in the smallest ***c*-P6** nanoring the exciton radiative rate is significantly suppressed[19] due to the circular symmetry of the lowest excited state, with the majority of the PL arising from dynamic symmetry breaking via Herzberg–Teller coupling.[4] As the molecules increase in size, the emissive rate for the nanorings tend toward the value of their linear counterparts. For the largest rings, the wave function may no longer be delocalized around the whole ring circumference,[5] leading to the exciton experiencing an effectively linear chain environment.[3] In the intermediate regime, a variety of processes may account for excitons appearing to have a larger radiative rate than naively expected (from the Kasha model), for instance, static or dynamic symmetry breaking[5] or thermal population of higher lying states with more closely spaced energy levels[33] for the larger rings.

There is negligible change in the radiative rate for the linear oligomers over the range of molecule lengths studied. While an increase in radiative rate with oligomer length has been

dx.doi.org/10.1021/jz5022153 | J. Phys. Chem. Lett. 2014, 5, 4356–4361

observed for shorter oligomers,[5,27] this effect is static over the presented size regime because the emissive exciton is limited in size and does not sample the whole molecule. It is noted that, while close, the radiative rates for the nanorings and oligomers do not tend to the same asymptote. A topological origin of this effect may be ruled out (see the Supporting Information for details); a structural cause is most likely, as the presence of an end group on a linear chain is expected to slightly perturb the emitting state.

To gain further insight into the anisotropy values measured for the samples, we perform a simulation of molecular conformation and exciton dynamics. Both the anisotropy dynamics and radiative rate may be qualitatively described by exciton generation, self-localization, and diffusion processes. A quantitative description requires knowledge of the molecule conformation, the initial and final exciton sizes, and the specific exciton migration process. The conformation for both linear and cyclic molecules in solution is expected to deviate from the idealized gas-phase shape predicted by naïve energy minimization; we have previously shown that nanorings adopt an open circular conformation with a range of elliptical distortions using small-angle X-ray scattering[15,16] and scanning tunnelling microscopy.[17] For the linear molecules, a typical chain is generated using the Monte Carlo random-walk approach described in refs 32 and 34. For the nanorings, typical conformations are generated using the Metropolis Markov-chain approach (and parameters) introduced in ref 35. A full account of details associated with the model is provided in the Supporting Information.

One method of estimating the initial size of the exciton is the "effective conjugation length" approach of Meier,[21] wherein a fit to a plot of peak absorption energy against $1/N$ is used. (See Figure 1d.) For the presented linear molecules, an initial effective conjugation length of ∼20 porphyrin units is calculated, which is also used for the cyclic molecules. While other metrics exist,[22] we find that the values generated by the Meier method give a good fit between simulation and experimental data. The final size of the exciton (after self-localization) is less easily calculated. Within the Kasha model, the radiative rate for a linear chain is expected to increase with chain length up to the emitting exciton size; we have previously shown that this is observed for oligomers of up to six units,[5] suggesting that the emissive exciton is limited in size to six or fewer units. The relationship between the initial anisotropy value and linear molecule length can also be used to estimate the emissive state size; this value is expected to remain constant for chains longer than the final state size. The initial anisotropy saturates at a lower bound for oligomers of between four and seven porphyrin units (5.4−9.5 nm[24]), as shown in Figure 2. These values for the relaxed exciton size are comparable to those previously measured, for instance seven units (∼5.5 nm[36]) for thiophene-based polymers as used by Westenhoff and colleagues[32] or four units (∼3 nm[37]) for the more weakly coupled bacteriochlorophyll monomers in natural light-harvesting system LH2 determined by Pullerits et al.[38] For the following modeling, a value of six repeat units is used; however, the modeling is not highly sensitive to the choice of this parameter within the four to seven range.

A line-dipole model is used to describe the exciton wave function, Ψ_k, where $\Psi_k = \sum_i a_k(i)\phi_i$.[39] Here k is an index over the exciton energy levels, $a_k(i)$ is an amplitude prefactor, and ϕ_i is a exciton subdipole wave function localized on the ith porphyrin unit. We restrict ourselves to considering the lowest ($k = 0$) exciton energy level for simplicity. The wave function may be generated in one of two ways; for the fully delocalized nanoring states, the exciton is divided between all sites with equal amplitude ($a(i)$ = constant), while for localized states, a sine function (such as used for describing the lowest energy wave function for a 1D particle-in-a-box) is used, where

$$a(i) = \frac{\sin[\pi(i - 0.5)/(n + 1)]}{\sum_{a=1}^{n} \sin[\pi a/(n + 1)]} \tag{2}$$

Here n is the length of the conjugated region enumerated in porphyrin monomer units; the 0.5 offset is used to place exciton amplitude on n monomer units. We randomly place an exciton on the generated molecular conformation which is then allowed to self-localize and migrate. Self-localization is simply modeled by an ultrafast reduction in size of the exciton, while migration is simulated using a simple 1D diffusion model with an exciton diffusion constant of 2 units^2/ps (corresponding to ∼3 nm^2/ps) obtained using an iterative optimization procedure. Here, we refer to on-chain migration as opposed to the combination of intra- and interchain migration typical of solid state polymer films.[40] An ensemble anisotropy value can then be calculated assuming a random orientation of the molecule by use of[28]

$$\gamma = \frac{3}{5}[(|\sum_i a_{\mathrm{ini}}(i)\hat{\varphi}_i|\cdot|\sum_i a_f(i)\hat{\varphi}_i|)^2 - 1] \tag{3}$$

where n is an index over the porphyrin sites, a_{ini} and a_f are strength distributions for the initial and final exciton wave function and $\hat{\varphi}_i$ is the vector describing the dipole subunit orientation at each point. We generate 300 conformations for each studied molecule and simulate 50 exciton creations for each conformation to produce an average anisotropy dynamic. Figure 4 shows a typical simulated molecule conformation with selected initial and final exciton wave functions along with experimental and averaged simulated anisotropy for four key cases. We emphasize that the primary input parameters to the simulation are independently determined, such as the initial and final exciton size and porphyrin-porphyrin bond bending constant (used in the Metropolis model[35]), with the exception of (i) the disorder parameter for the linear chain and (ii) the exciton diffusion constant which were both chosen for a good fit to the data. (Simulation results for all molecules used in this study are given in the Supporting Information.)

The absolute values and dynamics generated by our model agree remarkably well with the experimental values for polarization anisotropy, while simulated dipole strengths (see Supporting Information) qualitatively mirror the experimental values in Figure 3. The smallest nanoring (***c*-P6**) exhibits initial anisotropy values of $\gamma \leq 0.1$, arising from a fully delocalized absorbing and emitting state, in agreement with recent descriptions of its emission spectrum in terms of dynamic symmetry breaking (via the Herzberg−Teller mechanism).[4] The largest nanoring (***c*-P40**) cannot support a fully delocalized exciton state, leading to anisotropy dynamics qualitatively resembling its linear counterpart ***l*-P42**. Interestingly, the anisotropy decay for ***c*-P40** is notably quicker than for ***l*-P42**: the cyclic constraint requires the chain to curve more strongly, leading to a faster decay for a given molecular size. Intermediate nanorings (***c*-P10** and ***c*-P20**) are unlikely to support fully delocalized emissive states but retain ultrafast anisotropy loss because of a delocalized absorbing state which effectively randomizes the relative orientation of the absorbing and

dx.doi.org/10.1021/jz5022153 | J. Phys. Chem. Lett. 2014, 5, 4356−4361

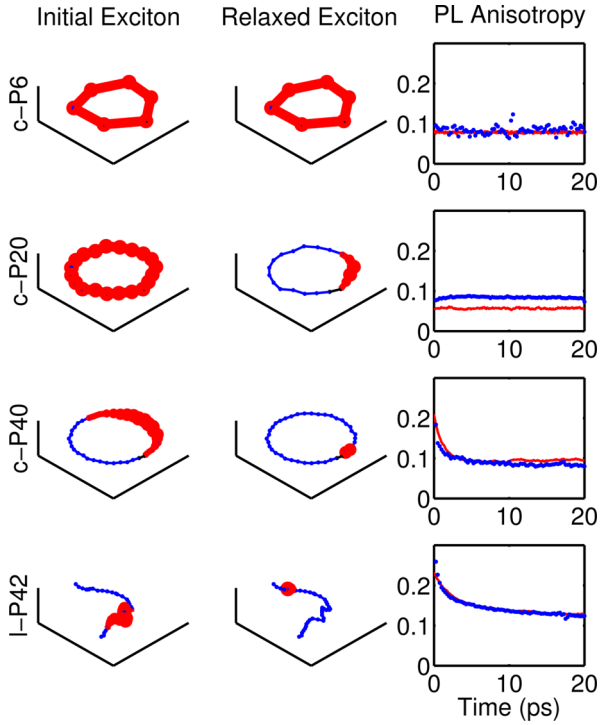

Figure 4. Schematic depicting a simulated molecular structure (blue line and points, representing the porphyrin centroid position) and exciton wave function (red) for four molecules. (Left) The initially excited exciton wave function and (center) the exciton wave function after localization and migration are shown. (Right) The experimental (blue points and line) and simulated (red line) anisotropy are plotted using the model described in the text. Results are shown for (from top to bottom) ***c*-P6**, ***c*-P20**, ***c*-P40**, and ***l*-P42** molecules.

emitting state. Interestingly, the model underestimates the anisotropy for these intermediate cases; it is likely that while such randomization occurs, certain sites are preferred due to the local energetic environment, as discussed by Aggarwal and colleagues.[3] The present model does not take into account quantum coherence,[13,41] static distortion[42] or breaks in conjugation,[31] due to the computational challenges arising from a full quantum-chemical treatment.

In conclusion, we have shown that exciton dynamics depend critically on both molecular size and shape. We demonstrate that a fully delocalized absorbing state persists to surprisingly large nanoring sizes, highlighting the use of such strongly coupled cyclic structures in quantum coherent[43] or light-harvesting applications.[12] For the largest nanoring sizes, both the absorbing and emitting state become localized resulting in radiative rates and lower anisotropy limits that approach the values measured for their linear counterparts. However, the dynamic decay of the polarization anisotropy in the cyclic structures remains faster than in their linear equivalents. In other words, while the quantum state described by the exciton wave function on the largest nanorings tends toward that on linear conjugated molecules, the later time evolution of the excitation continues to depend on the macrostructure of the system revealing a difference in the topology of the molecule. Our work therefore reveals that the fundamental issue of "ring-like" molecular behavior is governed by both quantum-mechanical and conformation limits.

■ ASSOCIATED CONTENT

Ⓢ Supporting Information

Synthesis and characterization details of all new compounds. Absorption and steady-state PL. Effective conjugation length calculations. PL lifetime and quantum efficiency. Example time-resolved PL, anisotropy and experimental details. Simulation details and extended results. This material is available free of charge via the Internet at http://pubs.acs.org.

■ AUTHOR INFORMATION

Corresponding Authors

*E-mail: p.parkinson1@physics.ox.ac.uk.
*E-mail: l.herz1@physics.ox.ac.uk.

Notes

The authors declare no competing financial interest.

■ ACKNOWLEDGMENTS

We thank the EPSRC (grant EP/J007161/1) and the ERC for support. We thank the National Mass Spectrometry Facility (Swansea) for mass spectra.

■ REFERENCES

(1) Montgomery, N. A.; Denis, J. C.; Schumacher, S.; Ruseckas, A.; Skabara, P. J.; Kanibolotsky, A.; Paterson, M. J.; Galbraith, I.; Turnbull, G. A.; Samuel, I. D. W. Optical Excitations in Star-Shaped Fluorene Molecules. *J. Phys. Chem. A* **2011**, *115*, 2913−2919.

(2) Chang, M. H.; Hoffmann, M.; Anderson, H. L.; Herz, L. M. Dynamics of Excited-State Conformational Relaxation and Electronic Delocalization in Conjugated Porphyrin Oligomers. *J. Am. Chem. Soc.* **2008**, *130*, 10171−10178.

(3) Aggarwal, A. V.; Thiessen, A.; Idelson, A.; Kalle, D.; Wursch, D.; Stangl, T.; Steiner, F.; Jester, S. S.; Vogelsang, J.; Hoger, S.; et al. Fluctuating Exciton Localization in Giant π-Conjugated Spoked-Wheel Macrocycles. *Nat. Chem.* **2013**, *5*, 964−970.

(4) Sprafke, J. K.; Kondratuk, D. V.; Wykes, M.; Thompson, A. L.; Hoffmann, M.; Drevinskas, R.; Chen, W.; Yong, C. K.; Kärnbratt, J.; Bullock, J. E.; et al. Belt-Shaped π-Systems: Relating Geometry to Electronic Structure in a Six-Porphyrin Nanoring. *J. Am. Chem. Soc.* **2011**, *133*, 17262−17273.

(5) Yong, C. K.; Parkinson, P.; Kondratuk, D. V.; Chen, W. H.; Stannard, A.; Summerfield, A.; Sprafke, J. K.; O'Sullivan, M. C.; Beton, P. H.; Anderson, H. L.; et al. Ultrafast Delocalization of Excitation in Synthetic Light-Harvesting Nanorings. *Chem. Sci.* **2015**, DOI: 10.1039/C4SC02424A.

(6) Kondratuk, D. V.; Perdigão, L. M. A.; Esmail, A. M. S.; O'Shea, J. N.; Beton, P. H.; Anderson, H. L., In Review.

(7) Kasha, M.; Rawls, H. R.; Ashraf El Bayoumi, M. The Exciton Model in Molecular Spectroscopy. *Pure Appl. Chem.* **1965**, *11*, 371−392.

(8) Kasha, M. Energy Transfer Mechanisms and the Molecular Exciton Model for Molecular Aggregates. *Radiat. Res.* **1963**, *20*, 55.

(9) Spano, F. C. The Spectral Signatures of Frenkel Polarons in H- and J-Aggregates. *Acc. Chem. Res.* **2010**, *43*, 429−439.

(10) Tempelaar, R.; Stradomska, A.; Knoester, J.; Spano, F. C. Anatomy of an Exciton: Vibrational Distortion and Exciton Coherence in H- and J-Aggregates. *J. Phys. Chem. B* **2013**, *117*, 457−466.

(11) Selinger, B. K.; Ware, W. R. Fluorescence Lifetime of Benzene and Benzene-d_6 Vapor Excited to Single Vibronic Levels. *J. Chem. Phys.* **1970**, *53*, 3160−3168.

(12) Cogdell, R. J.; Gall, A.; Kohler, J. The Architecture and Function of the Light-Harvesting Apparatus of Purple Bacteria: from Single Molecules to *in vivo* Membranes. *Q. Rev. Biophys.* **2006**, *39*, 227−324.

(13) Hildner, R.; Brinks, D.; Nieder, J. B.; Cogdell, R. J. Quantum Coherent Energy Transfer over Varying Pathways in Single Light-Harvesting Complexes. *Science* **2013**, *340*, 1448−1451.

(14) Fleming, G. R.; Scholes, G. D. Physical Chemistry - Quantum Mechanics for Plants. *Nature* **2004**, *431*, 256−257.
(15) O'Sullivan, M. C.; Sprafke, J. K.; Kondratuk, D. V.; Rinfray, C.; Claridge, T. D. W.; Saywell, A.; Blunt, M. O.; O'Shea, J. N.; Beton, P. H.; Malfois, M.; et al. Vernier Templating and Synthesis of a 12-Porphyrin Nano-ring. *Nature* **2011**, *469*, 72−75.
(16) Kondratuk, D. V.; Sprafke, J. K.; O'Sullivan, M. C.; Perdigao, L. M. A.; Saywell, A.; Malfois, M.; O'Shea, J. N.; Beton, P. H.; Thompson, A. L.; Anderson, H. L. Vernier-Templated Synthesis, Crystal Structure, and Supramolecular Chemistry of a 12-Porphyrin Nanoring. *Chem.—Eur. J.* **2014**, *20*, 12826.
(17) Kondratuk, D. V.; Perdigao, L. M. A.; Sullivan, M. C. O.; Svatek, S.; Smith, G.; Shea, J. N. O.; Beton, P. H.; Anderson, H. L. Two Vernier-Templated Routes to a 24-Porphyrin Nanoring. *Angew. Chem., Int. Ed.* **2012**, *51*, 6696−6699.
(18) Parkinson, P.; Knappke, C. E. I.; Kamonsutthipaijit, N.; Sirithip, K.; Matichak, J. D.; Anderson, H. L.; Herz, L. M. Ultrafast Energy Transfer in Biomimetic Multistrand Nanorings. *J. Am. Chem. Soc.* **2014**, *136*, 8217−8220.
(19) Hoffmann, M.; Kärnbratt, J.; Chang, M. H.; Herz, L. M.; Albinsson, B.; Anderson, H. L. Enhanced π Conjugation Around a Porphyrin[6] Nanoring. *Angew. Chem., Int. Ed.* **2008**, *120*, 5071.
(20) Williams, V. E.; Swager, T. M. An Improved Synthesis of Poly(p-phenylenebutadiynylene)s. *J. Polym. Sci., Polym. Chem.* **2000**, *38*, 4669−4676.
(21) Meier, H.; Stalmach, U.; Kolshorn, H. Effective Conjugation Length and UV/Vis Spectra of Oligomers. *Acta Polym.* **1997**, *48*, 379−384.
(22) Gierschner, J.; Cornil, J.; Egelhaaf, H. J. Optical Bandgaps of π-Conjugated Organic Materials at the Polymer Limit: Experiment and Theory. *Adv. Mater.* **2007**, *19*, 173−191.
(23) Zade, S. S.; Zamoshchik, N.; Bendikov, M. From Short Conjugated Oligomers to Conjugated Polymers. Lessons from Studies on Long Conjugated Oligomers. *Acc. Chem. Res.* **2011**, *44*, 14−24.
(24) Taylor, P. N.; Huuskonen, J.; Rumbles, G.; Aplin, R. T.; Williams, E.; Anderson, H. L. Conjugated Porphyrin Oligomers from Monomer to Hexamer. *Chem. Commun.* **1998**, 909.
(25) McCulloch, B.; Ho, V.; Hoarfrost, M.; Stanley, C.; Do, C.; Heller, W. T.; Segalman, R. A. Polymer Chain Shape of Poly(3-alkylthiophenes) in Solution using Small-Angle Neutron Scattering. *Macromolecules* **2013**, *46*, 1899−1907.
(26) Lin, V. S. Y.; Therien, M. J. The Role of Porphyrin-to-Porphyrin Linkage Topology in the Extensive Modulation of the Absorptive and Emissive Properties of a Series of Ethynyl- and Butadiynyl-Bridged Bis- and Tris(porphinato)zinc Chromophores. *Chem.—Eur. J.* **1995**, *1*, 645−651.
(27) Duncan, T. V.; Susumu, K.; Sinks, L. E.; Therien, M. J. Exceptional Near-Infrared Fluorescence Quantum Yields and Excited-State Absorptivity of Highly Conjugated Porphyrin Arrays. *J. Am. Chem. Soc.* **2006**, *128*, 9000−9001.
(28) Valeur, B.; Berberan-Santos, M. N. *Molecular Fluorescence: Principles and Applications*; John Wiley & Sons: Chichester, U.K., 2012.
(29) Chang, M. H.; Frampton, M. J.; Anderson, H. L.; Herz, L. M. Intermolecular Interaction Effects on the Ultrafast Depolarization of the Optical Emission from Conjugated Polymers. *Phys. Rev. Lett.* **2007**, *98*, 027402.
(30) Galli, C.; Wynne, K.; LeCours, S. M.; Therien, M. J.; Hochstrasser, R. M. Direct Measurement of Electronic Dephasing using Anisotropy. *Chem. Phys. Lett.* **1993**, *206*, 493−499.
(31) Ruseckas, A.; Wood, P.; Samuel, I. D. W.; Webster, G. R.; Mitchell, W. J.; Burn, P. L.; Sundström, V. Ultrafast Depolarization of the Fluorescence in a Conjugated Polymer. *Phys. Rev. B* **2005**, *72*, 115214.
(32) Westenhoff, S.; Beenken, W. J. D.; Yartsev, A.; Greenham, N. C. Conformational Disorder of Conjugated Polymers. *J. Chem. Phys.* **2006**, *125*, 154903.
(33) Feldmann, J.; Peter, G.; Göbel, E. O.; Dawson, P.; Moore, K.; Foxon, C.; Elliott, R. J. Linewidth Dependence of Radiative Exciton Lifetimes in Quantum Wells. *Phys. Rev. Lett.* **1987**, *59*, 2337−2340.
(34) Grage, M. M. L.; Wood, P. W.; Ruseckas, A.; Pullerits, T.; Mitchell, W.; Burn, P. L.; Samuel, I. D. W.; Sundström, V. Conformational Disorder and Energy Migration in MEH-PPV with Partially Broken Conjugation. *J. Chem. Phys.* **2003**, *118*, 7644−7650.
(35) Svatek, S. A.; Perdigao, L. M. A.; Stannard, A.; Wieland, M. B.; Kondratuk, D. V.; Anderson, H. L.; O'Shea, J. N.; Beton, P. H. Mechanical Stiffening of Porphyrin Nanorings Through Supramolecular Columnar Stacking. *Nano Lett.* **2013**, *13*, 3391−3395.
(36) Prosa, T. J.; Winokur, M. J.; Moulton, J.; Smith, P.; Heeger, A. J. X-ray Structural Studies of Poly(3-alkylthiophenes) - an Example of an Inverse Comb. *Macromolecules* **1992**, *25*, 4364−4372.
(37) McDermott, G.; Prince, S. M.; Freer, A. A.; Hawthornthwaite-Lawless, A. M.; Papiz, M. Z.; Cogdell, R. J.; Isaacs, N. W. Crystal-Structure of an Integral Membrane Light-Harvesting Complex from Photosynthetic Bacteria. *Nature* **1995**, *374*, 517−521.
(38) Pullerits, T.; Chachisvilis, M.; Sundström, V. Exciton Delocalization Length in the B850 Antenna of Rhodobacter Sphaeroides. *J. Phys. Chem.* **1996**, *100*, 10787.
(39) Beenken, W. J. D.; Pullerits, T. Excitonic Coupling in Polythiophenes: Comparison of Different Calculation Methods. *J. Chem. Phys.* **2004**, *120*, 2490.
(40) Beljonne, D.; Pourtois, G.; Silva, C.; Hennebicq, E.; Herz, L. M.; Friend, R. H.; Scholes, G. D.; Setayesh, S.; Müllen, K.; Bredas, J. L. Interchain vs. Intrachain Energy Transfer in Acceptor-Capped Conjugated Polymers. *Proc. Natl. Acad. Sci. U. S. A.* **2002**, *99*, 10982−10987.
(41) Kuhn, O.; Sundström, V.; Pullerits, T. Fluorescence Depolarization Dynamics in the B850 Complex of Purple Bacteria. *Chem. Phys.* **2002**, *275*, 15−30.
(42) Ketelaars, M.; Matsushita, M.; Kohler, J.; Schmidt, J.; Aartsma, T. J. Spectroscopy on the B850 Band of Individual Light-Harvesting 2 Complexes of Rhodopseudomonas Acidophila i. Experiments and Monte Carlo Simulations. *Biophys. J.* **2001**, *80*, 1591−1603.
(43) Govorov, A. O.; Ulloa, S. E.; Karrai, K.; Warburton, R. J. Polarized Excitons in Nanorings and the Optical Aharonov-Bohm Effect. *Phys. Rev. B* **2002**, *66*, 081309.